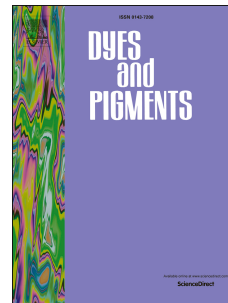


# Accepted Manuscript

Effect of structural modification on the performances of phenothiazine-dye sensitized solar cells

Xuxu Liu, Jun Long, Guo Wang, Yong Pei, Bin Zhao, Songting Tan



PII: S0143-7208(15)00183-7

DOI: [10.1016/j.dyepig.2015.05.012](https://doi.org/10.1016/j.dyepig.2015.05.012)

Reference: DYPI 4775

To appear in: *Dyes and Pigments*

Received Date: 8 January 2015

Revised Date: 31 March 2015

Accepted Date: 11 May 2015

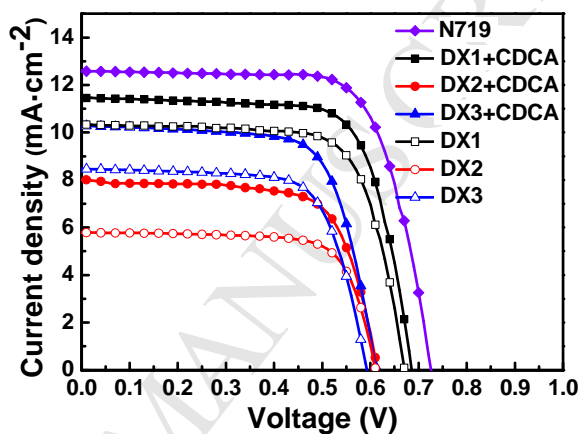
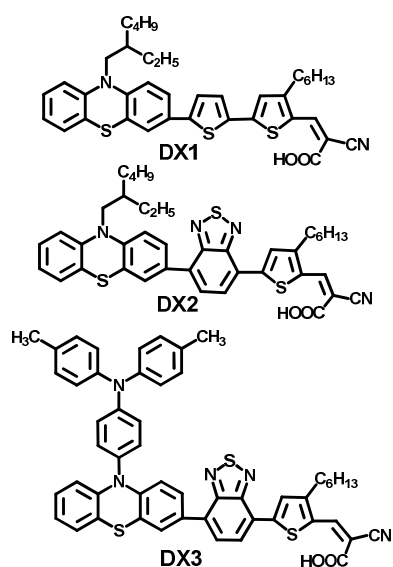
Please cite this article as: Liu X, Long J, Wang G, Pei Y, Zhao B, Tan S, Effect of structural modification on the performances of phenothiazine-dye sensitized solar cells, *Dyes and Pigments* (2015), doi: 10.1016/j.dyepig.2015.05.012.

This is a PDF file of an unedited manuscript that has been accepted for publication. As a service to our customers we are providing this early version of the manuscript. The manuscript will undergo copyediting, typesetting, and review of the resulting proof before it is published in its final form. Please note that during the production process errors may be discovered which could affect the content, and all legal disclaimers that apply to the journal pertain.

## Graphical Abstract

## Effect of structural modification on the performances of phenothiazine-dye sensitized solar cells

Xuxu Liu, Jun Long, Guo Wang, Yong Pei, Bin Zhao, Songting Tan



## Effect of structural modification on the performances of phenothiazine-dye sensitized solar cells

Xuxu Liu<sup>a</sup>, Jun Long<sup>a</sup>, Guo Wang<sup>a</sup>, Yong Pei<sup>a</sup>, Bin Zhao<sup>a,b</sup>, Songting Tan<sup>a,b,\*</sup>

<sup>a</sup> College of Chemistry, and Key Laboratory of Environmentally Friendly Chemistry and Applications of Ministry of Education, Xiangtan University, Xiangtan 411105, PR China

<sup>b</sup> Key Laboratory of Advanced Functional Polymeric Materials of College of Hunan Province, Key Laboratory of Polymeric Materials & Application Technology of Hunan Province, Xiangtan University, Xiangtan 411105, PR China

\* Corresponding author. *E-mail address:* [tanst2008@163.com](mailto:tanst2008@163.com) (S. Tan).

**ABSTRACT:** Three novel dyes **DX1**, **DX2** and **DX3** containing phenothiazine are designed and synthesized for dye-sensitized solar cells (DSSCs). Photophysical, electrochemical and photovoltaic properties of the three dyes have been systematically investigated. The results show that the **DX1**-based DSSC with 0.5 mM chenodeoxycholic acid (CDCA) obtains the power conversion efficiency (PCE) of 5.69%. When an additional electron-deficient benzothiadiazole (BT) unit is introduced into the molecular structures of the dyes **DX2** and **DX3**, the absorption spectra are broadened. But the short-circuit photocurrent density ( $J_{sc}$ ) of the devices are decreased due to the blocked electron transfer, so the DSSC device based on **DX2** only obtains the PCE of 3.43%. Furthermore, a triphenylamine (TPA) unit with high electron-donating ability is joined onto the nitrogen atom of phenothiazine donor in **DX3**, which enhances the electron injection efficiency and reduces the dye aggregation. Thus, the  $J_{sc}$  is improved, resulting in a higher PCE of 4.41% in the **DX3**-based dye than the **DX2**-based one.

Key words: dye-sensitized solar cells, phenothiazine, benzothiadiazole, photovoltaic performances, synthesis

## 1. Introduction

As a promising alternative to conventional inorganic photovoltaic devices, dye-sensitized solar cells (DSSCs) have drawn much attention since their introduction in 1991 [1], due to their potentially low-cost fabrication, possibility of transparency and color selectivity, which can be integrated into building and automobile applications [2-5]. As is well-known, the sensitizer is always a crucial element in DSSCs, exerting a significant influence on the power conversion efficiency (PCE) as well as the device stability. To date, DSSCs incorporating ruthenium based dyes and zinc-porphyrin based co-dyes have reached high efficiency over 11% [6,7], and 12% [8,9], respectively. Thereinto, a new dye based on zinc-porphyrin, SM315, which was reported by Grätzel *et al.*, showed a record PCE of 13.0% [10]. However, metal-free organic dyes, commonly constructed with donor- $\pi$  bridge-acceptor (D- $\pi$ -A) configuration, have become increasingly attractive for the merits of high molar extinction coefficients, low cost, environment-friendly property and high flexibility of molecular design [6,11]. Thus, some dyes such as triphenylamine- (TPA-), carbazole-, phenothiazine-, and indoline-based ones have achieved relatively high PCEs by using iodide/triiodide-based electrolytes [12-21]. However, most of the D- $\pi$ -A dyes tend to form intermolecular aggregation on the TiO<sub>2</sub> surface, which affects the light absorption and loss in the photo-generated electrons. Therefore, further studies are needed to develop new dyes to maximize the electron accumulation in the TiO<sub>2</sub> conduction band, reduce the charge recombination and absorb light intensely in the red to near-infrared (NIR) region, which accounts for about 50% of solar energy [22-23].

Phenothiazine-based dyes have been intensively explored in recent years. In phenothiazine system, two phenyl groups are arranged with a small torsion angle related to the nitrogen and sulfur atoms, ensuring that the  $\pi$ -delocalization can be extended over the entire chromophore [24-29]. Meanwhile, attaching a bulky or branched alkyl chain to the nitrogen atom of phenothiazine unit lead to the non-planar butterfly conformation of phenothiazine,

which can sufficiently inhibit molecular aggregation and further enhance the charge separation on the TiO<sub>2</sub> interface [30,31]. Furthermore, a new type of dyes with an additional electron-deficient unit introduced between the donor and  $\pi$ -bridge have been designed and characterized as a D-A- $\pi$ -A architecture [32]. In the novel D-A- $\pi$ -A configuration dyes, the additional acceptor chromophore, which extends the range of  $\pi$ -electron delocalization, can facilitate intramolecular charge transfer and adjust the band gap for harvesting more near-infrared (NIR) light [33]. Among all the additional electron-deficient units, benzothiadiazole (BT) has been one of the most widely utilized in DSSCs [34-38]. Here, we designed and synthesized three novel dyes (**DX1**, **DX2** and **DX3**, Scheme 1), which contained phenothiazine donors and cyanoacrylic acid acceptors bridged by a 3-hexylthiophene unit as a  $\pi$ -spacer. Additionally, a BT unit was applied as an additional acceptor into the dyes **DX2** and **DX3** to realize a broadened absorption spectrum. Notably, the 3D nonplanar TPA [39,40] was introduced to the 10-position nitrogen atom of phenothiazine donor in **DX3** to obtain a double-donor structure, which resulted in enhanced electron-donating ability and reduced dye aggregation. Photophysical, electrochemical and photovoltaic properties of the three dyes were systematically investigated.

## 2. Experimental section

### 2.1. Materials

All the chemicals were purchased from Alfa Aesar and Chem Greatwall Chemical Company (Wuhan, China) and used without further purification. Toluene and tetrahydrofuran (THF) were dried and distilled over sodium and benzophenone. N,N-Dimethylformamide (DMF) was dried over and distilled from CaH<sub>2</sub> under an atmosphere of dry nitrogen. Phosphorus oxychloride and 1,2-dichloroethane were atmospheric distillation. All other commercially available materials were used as received unless noted otherwise.

4-Bromo-7-(4-hexylthiophen-2-yl)benzo[*c*][1,2,5]thiadiazole (5) [41],

3-bromo-10-(2-ethylhexyl)-10H-phenothiazine (7) [42] were prepared according to literature procedures.

## 2.2. Synthesis

The synthetic routes and molecular structures of the dyes are shown in Scheme 1. The detailed synthetic processes are as follows.

### 2.2.1. 2-Bromo-4-hexylthiophene (1)

A solution of 3-hexylthiophene (8.00 g, 47.53 mmol) in anhydrous THF (100 mL) was cooled down to  $-78\text{ }^{\circ}\text{C}$  under argon atmosphere, and *n*-BuLi (2.5 M in hexane, 22.82 mL, 57.04 mmol) was added dropwise. After stirring for 3 h, carbon tetrabromide (18.92 g, 57.04 mmol) in anhydrous THF (30 mL) was added dropwise and the reaction medium was slowly warmed to the room temperature. Water was added for quenching the reaction, and the solution was extracted with  $\text{CH}_2\text{Cl}_2$ . The organic layer was washed with  $\text{H}_2\text{O}$  and dried over  $\text{MgSO}_4$ . Solvent was removed by rotary evaporation. The crude product was purified on silica gel column chromatography with petroleum ether to get a yellow liquid (11.50 g, 97.9%).  $^1\text{H NMR}$  ( $\text{CDCl}_3$ , 400MHz,  $\delta/\text{ppm}$ ): 6.88 (s, 1H), 6.80 (s, 1H), 2.56–2.53 (t, 2H,  $J = 7.5\text{ Hz}$ ), 1.29–1.26 (m, 8H), 0.89–0.87 (t, 3H,  $J = 6.2\text{ Hz}$ ). GC-MS ( $\text{C}_{10}\text{H}_{15}\text{BrS}$ )  $m/z$ : calcd for 247.2; found 248.0.

### 2.2.2. 5-Bromo-3-hexylthiophene-2-carbaldehyde (2)

The compound **2** was synthesized by Vilsmeier reaction. Under nitrogen atmosphere, to a solution of compound **1** (11.50 g, 46.52 mmol) in dichloroethane (100 mL), anhydrous DMF (4.32 mL, 55.83 mmol) and  $\text{POCl}_3$  (5.20 mL, 55.83 mmol) was added slowly at  $0\text{ }^{\circ}\text{C}$ . The mixture was stirred at  $0\text{ }^{\circ}\text{C}$  for 20 min and then heated to  $85\text{ }^{\circ}\text{C}$  for 24 h. After cooled to room temperature, sodium acetate solution (50 mL) was added to hydrolyse the reaction for 4 hours. Then the mixture was extracted with  $\text{CH}_2\text{Cl}_2$  and washed with water. The organic phase was dried over anhydrous

MgSO<sub>4</sub> and the solvent was removed by rotary evaporation. The crude product was purified on silica gel chromatography using a petroleum ether/ dichloromethane mixture (1/1 by volume) as eluent to afford a yellow liquid (5.21 g, 40.7%). <sup>1</sup>H NMR (CDCl<sub>3</sub>, 400MHz, δ/ppm): 9.92 (s, 1H), 6.85 (s, 1H), 2.90–2.86 (t, 2H, *J* = 7.6 Hz), 1.66–1.25 (m, 8H), 0.89–0.87 (t, 3H, *J* = 6.3 Hz). GC-MS (C<sub>11</sub>H<sub>15</sub>BrOS) *m/z*: calcd for 275.2; found 276.0.

### 2.2.3. 4-Hexyl-[2,2'-bithiophene]-5-carbaldehyde (**3**)

The compound **3** was synthesized by Stille coupling reaction. Compound **2** (1.50 g, 5.45 mmol) and tributyl(thiophen-2-yl)stannane (3.05 g, 8.18 mmol) were dissolved in anhydrous toluene (40 mL) and deoxygenated with nitrogen for 15 min. Pd(PPh<sub>3</sub>)<sub>4</sub> (190 mg, 0.17 mmol) was then added under nitrogen and the mixture was again flushed with nitrogen for 30 min. Then the reaction mixture was stirred at 110 °C for 2 days under nitrogen atmosphere. After cooled to room temperature, the mixture was poured into water (50 mL) and extracted with dichloromethane. The organic phase was washed with water and dried over anhydrous MgSO<sub>4</sub>. After concentration, the crude product was purified on silica gel chromatography using a petroleum ether/dichloromethane mixture (2/1 by volume) as eluent to afford an orange liquid (1.51 g, 98.6%). <sup>1</sup>H NMR (CDCl<sub>3</sub>, 400MHz, δ/ppm): 9.99 (s, 1H), 7.35–7.34 (d, 2H, *J* = 3.4 Hz), 7.07–7.05 (d, 2H, *J* = 4.6 Hz), 2.95–2.91 (t, 2H, *J* = 7.7 Hz), 1.74–1.26 (m, 8H), 0.90 (s, 3H). GC-MS (C<sub>15</sub>H<sub>18</sub>OS<sub>2</sub>) *m/z*: calcd for 278.4; found 278.1.

### 2.2.4. 5'-Bromo-4-hexyl-[2,2'-bithiophene]-5-carbaldehyde (**4**)

Compound **3** (1.31 g, 4.70 mmol) was dissolved in DMF (20 mL). The mixture of N-bromosuccinimide (NBS) (1.00 g, 5.65 mmol) in DMF (15 mL) was added dropwise to the solution and the solution was stirred for 24 hours in the dark. Then, the mixture was poured into water and extracted with diethyl ether, then washed by water. The organic phase was dried over anhydrous MgSO<sub>4</sub>, and then the solvent was removed by rotary evaporation. The crude product was purified on silica gel chromatography using a petroleum ether/dichloromethane mixture (4/1 by volume) as

eluent to afford an orange liquid (1.18 g, 70.1%).  $^1\text{H}$  NMR ( $\text{CDCl}_3$ , 400MHz,  $\delta/\text{ppm}$ ): 9.99 (s, 1H), 7.08 (s, 1H), 7.03–7.02 (d, 1H,  $J = 3.4$  Hz), 6.99 (s, 1H), 2.94–2.90 (t, 2H,  $J = 7.5$  Hz), 1.70–1.26 (m, 8H), 0.90 (s, 3H). MALDI-TOF MS ( $\text{C}_{15}\text{H}_{17}\text{BrOS}_2$ )  $m/z$ : calcd for 357.329; found 357.078.

#### 2.2.5. 5-(7-Bromobenzo[*c*][1,2,5]thiadiazol-4-yl)-3-hexylthiophene-2-carbaldehyde (**6**)

The synthetic procedure for compound **6** was similar to that for compound **2**, except that compound **5** (3.00 g, 7.87 mmol) was used instead of compound **1**. The crude product was purified on silica gel chromatography using a petroleum ether/dichloromethane mixture (1/1 by volume) as eluent to afford a yellow solid (2.50 g, 78.1%).  $^1\text{H}$  NMR ( $\text{CDCl}_3$ , 400MHz,  $\delta/\text{ppm}$ ): 10.14 (s, 1H), 8.07 (s, 1H), 7.95–7.85 (d, 2H,  $J = 7.6$  Hz), 3.09–3.06 (t, 2H,  $J = 7.5$  Hz), 1.82–1.77 (m, 2H), 1.47 (s, 2H), 1.38 (s, 2H), 1.30 (s, 2H), 0.94 (s, 3H). MALDI-TOF MS ( $\text{C}_{17}\text{H}_{17}\text{BrN}_2\text{OS}_2$ )  $m/z$ : calcd for 409.364; found 409.077.

#### 2.2.6. 10-(2-Ethylhexyl)-3-(4,4,5,5-tetramethyl-1,3,2-dioxaborolane-2-yl)-10H-phenothiazine (**8**)

A solution of the compound **7** (7.99 g, 20.48 mmol) in anhydrous THF (40 mL) was cooled down to  $-78$  °C under argon atmosphere, and *n*-BuLi (2.5 M in hexane, 8.19 mL, 20.48 mmol) was added dropwise. After stirring for 3 h, 2-isopropoxy-4,4,5,5-tetramethyl-1,3,2-dioxaborolane (4.18 mL, 20.48 mmol) was added dropwise and the reaction medium was slowly warmed to the room temperature. Water was added for quenching the reaction, and the aqueous layer was then extracted with  $\text{CH}_2\text{Cl}_2$ . The organic layer was washed with  $\text{H}_2\text{O}$  and dried over  $\text{MgSO}_4$ . Solvent was removed by rotary evaporation. The crude product was purified on silica gel column chromatography with a petroleum ether/ethyl acetate mixture (30:1 by volume) to afford a yellow-green oil (4.75 g, 53.0%).  $^1\text{H}$  NMR ( $\text{CDCl}_3$ , 400MHz,  $\delta/\text{ppm}$ ): 7.58 (s, 2H), 7.13–7.12 (d, 2H,  $J = 6.8$  Hz), 6.92–6.91 (d, 1H,  $J = 6.9$  Hz), 6.86–6.85 (m, 2H), 3.74–3.73 (d, 2H,  $J = 5.3$  Hz), 1.93–1.90 (m, 1H), 1.44–1.32 (m, 8H), 1.26 (s, 12H), 0.87–0.83 (t, 6H,  $J = 7.1$  Hz). MALDI-TOF MS ( $\text{C}_{26}\text{H}_{36}\text{BNO}_2\text{S}$ )  $m/z$ : calcd for 437.446; found 437.328.

### 2.2.7. 5'-(10-(2-Ethylhexyl)-10H-phenothiazin-3-yl)-4-hexyl-[2,2'-bithiophene]-5-carbaldehyde (**9**)

The compound **9** was synthesized by Suzuki reaction. Compound **8** (0.78 g, 1.79 mmol), compound **4** (0.53 g, 1.49 mmol), potassium carbonate (1.03 g, 7.45 mmol) dissolved in water (3 mL) and thimbleful tetrabutylammonium bromide (TBAB) were dissolved in anhydrous DMF (30 mL) and deoxygenated with nitrogen for 15 min. Pd(PPh<sub>3</sub>)<sub>4</sub> (52 mg, 0.045 mmol) was then added under nitrogen and the mixture was again flushed with nitrogen for 30 min. Then the reaction mixture was stirred at 100 °C for two days under nitrogen atmosphere. After cooled to room temperature, the mixture was poured into water (50 mL) and extracted with dichloromethane. The organic phase was washed with water and dried over anhydrous MgSO<sub>4</sub>. After concentration, the crude product was purified on silica gel chromatography using a petroleum ether/dichloromethane mixture (2/1 by volume) as eluent to afford an orange-red oil (0.86 g, 97.2%). <sup>1</sup>H NMR (CDCl<sub>3</sub>, 400MHz, δ/ppm): 9.98 (s, 1H), 7.39–7.37 (d, 2H, *J* = 6.3 Hz), 7.19–7.14 (m, 3H), 7.05 (s, 1H), 6.96–6.86 (m, 4H), 3.76–3.74 (d, 2H, *J* = 6.9 Hz), 2.95–2.91 (t, 2H, *J* = 7.6 Hz), 1.94 (m, 1H), 1.72–1.69 (m, 3H), 1.52–1.26 (m, 12H), 0.90–0.84 (m, 9H). <sup>13</sup>C NMR (100 MHz, CDCl<sub>3</sub>, δ/ppm): 181.27, 153.85, 146.12, 145.83, 145.23, 145.22, 135.59, 134.52, 127.99, 127.66, 127.36, 126.99, 126.57, 126.12, 125.11, 124.77, 124.56, 123.21, 122.75, 116.10, 116.05, 51.21, 36.07, 31.60, 31.31, 30.81, 29.04, 28.65, 28.61, 24.14, 23.09, 22.59, 14.09, 14.03, 10.58. MALDI-TOF MS (C<sub>35</sub>H<sub>41</sub>NOS<sub>3</sub>) *m/z*: calcd for 587.901; found 587.309.

### 2.2.8.

### 5-(7-(10-(2-Ethylhexyl)-10H-phenothiazin-3-yl)benzo[*c*][1,2,5]thiadiazol-4-yl)-3-hexylthiophene-2-carbaldehyde (**10**)

The synthetic procedure for compound **10** was similar to that for compound **9**, except that compound **6** (0.80 g, 1.95 mmol) was used instead of compound **4**. The crude product was purified on silica gel chromatography using a petroleum ether/dichloromethane mixture (2/1 by volume) as eluent to afford a black red solid (1.09 g, 85.2%). <sup>1</sup>H

NMR (CDCl<sub>3</sub>, 400MHz,  $\delta$ /ppm): 10.10 (s, 1H), 8.06 (s, 1H), 8.01–7.99 (d, 1H,  $J = 7.4$  Hz), 7.85–7.82 (m, 2H), 7.70–7.69 (d, 1H,  $J = 7.4$  Hz), 7.20–7.16 (m, 2H), 7.03–7.01 (d, 1H,  $J = 8.3$  Hz), 6.97–6.91 (m, 2H), 3.81–3.80 (d, 2H,  $J = 6.8$  Hz), 3.06–3.02 (t, 2H,  $J = 7.5$  Hz), 2.02–1.99 (m, 1H), 1.79–1.74 (m, 2H), 1.54–1.30 (m, 14H), 0.92–0.89 (t, 9H,  $J = 7.0$  Hz). <sup>13</sup>C NMR (100 MHz, CDCl<sub>3</sub>,  $\delta$ /ppm): 182.03, 153.71, 153.27, 152.69, 147.60, 146.53, 145.19, 137.46, 133.59, 130.93, 130.53, 128.29, 128.02, 127.71, 127.38, 127.26, 126.55, 126.08, 125.44, 124.48, 122.75, 116.12, 115.76, 51.24, 36.09, 31.61, 31.45, 30.86, 29.07, 28.75, 28.67, 24.17, 23.09, 22.58, 14.04, 14.00, 10.56. MALDI-TOF MS (C<sub>37</sub>H<sub>41</sub>N<sub>3</sub>OS<sub>3</sub>) m/z: calcd for 639.936; found 639.298.

#### 2.2.9. 4-Iodo-N,N-di-p-tolylaniline (**11**)

A suspended solution of 4-methyl-N-phenyl-N-(p-tolyl)aniline (10.00 g, 36.59 mmol), iodine (3.99 g, 15.70 mmol), and periodic acid (1.49 g, 6.53 mmol) in 95% ethanol (10 mL) was refluxed under nitrogen for 4 h. The reaction mixture was cooled to room temperature and then saturated sodium subsulfite aqueous solution (50 mL) was added. The crude product was extracted into dichloromethane, washed with water, and dried over anhydrous sodium sulfate. After removing solvent under reduced pressure, the residue was purified on silica gel chromatography using petroleum ether as eluent to yield a white solid (12.66 g, 86.6%). <sup>1</sup>H NMR (CDCl<sub>3</sub>, 400MHz,  $\delta$ /ppm): 7.46–7.44 (d, 2H,  $J = 8.1$  Hz), 7.08–7.06 (d, 4H,  $J = 7.7$  Hz), 6.99–6.97 (d, 4H,  $J = 7.7$  Hz), 6.78–6.76 (d, 2H,  $J = 8.1$  Hz), 2.32 (s, 6H). MALDI-TOF MS (C<sub>20</sub>H<sub>18</sub>IN) m/z: calcd for 399.268; found 399.130.

#### 2.2.10. N-(4-(10H-phenothiazin-10-yl)phenyl)-4-methyl-N-(p-tolyl)aniline (**12**)

Compound **11** (10.00 g, 25.05 mmol), 10H-phenothiazine (4.16 g, 20.87 mmol), copper powder (0.80 g, 12.52 mmol) and potassium carbonate (4.32 g, 31.31 mmol) were mixed and stirred for 8 h at 180 °C, then after the mixture was cooled to 130 °C, ethyl acetate (30 mL) was added by means of a syringe, and the solution was stirred for 1 h. After the solution was cooled to room temperature, the solvent was removed by rotary evaporation. The crude

product was purified on silica gel chromatography using a petroleum ether/dichloromethane mixture (4/1 by volume) as eluent to afford a white powder (1.79 g, 18.2%).  $^1\text{H}$  NMR ( $\text{CDCl}_3$ , 400MHz,  $\delta/\text{ppm}$ ): 7.16–7.12 (m, 12H), 7.00–6.98 (d, 2H,  $J = 7.1$  Hz), 6.90–6.87 (m, 2H), 6.81–6.78 (m, 2H), 6.32–6.30 (d, 2H,  $J = 7.7$  Hz), 2.34 (s, 6H). MALDI-TOF MS ( $\text{C}_{32}\text{H}_{26}\text{N}_2\text{S}$ )  $m/z$ : calcd for 470.627; found 470.172.

#### 2.2.11. 4-(3-Bromo-10H-phenothiazin-10-yl)-N,N-di-p-tolylaniline (**13**)

The synthetic procedure for compound **13** was similar to that for compound **4**, except that compound **12** (1.79 g, 3.80 mmol) was used instead of compound **3**. The crude product was purified on silica gel chromatography using petroleum ether as eluent to afford a light green solid (1.49 g, 71.4%).  $^1\text{H}$  NMR ( $\text{CDCl}_3$ , 400MHz,  $\delta/\text{ppm}$ ): 7.14–7.08 (m, 13H), 6.97–6.87 (m, 3H), 6.82–6.80 (m, 1H), 6.30–6.29 (d, 1H,  $J = 7.4$  Hz), 6.16–6.14 (d, 1H,  $J = 8.5$  Hz), 2.34 (s, 6H). MALDI-TOF MS ( $\text{C}_{32}\text{H}_{25}\text{BrN}_2\text{S}$ )  $m/z$ : calcd for 549.523; found 550.154.

#### 2.2.12.

#### 4-Methyl-N-(p-tolyl)-N-(4-(3-(4,4,5-trimethyl-1,3,2-dioxaborolan-2-yl)-10H-phenothiazin-10-yl)phenyl)aniline (**14**)

The synthetic procedure for compound **14** was similar to that for compound **8**, except that compound **13** (0.71 g, 1.30 mmol) was used instead of compound **7**. The crude product was purified on silica gel column chromatography with a petroleum ether/ethyl acetate mixture (30:1 by volume) to obtain a yellow-green oil (0.57 g, 73.2%).  $^1\text{H}$  NMR ( $\text{CDCl}_3$ , 400MHz,  $\delta/\text{ppm}$ ): 7.39 (s, 1H), 7.30–7.28 (d, 1H,  $J = 8.3$  Hz), 7.14–7.11 (m, 12H), 6.96–6.94 (d, 1H,  $J = 7.3$  Hz), 6.87–6.83 (m, 1H), 6.80–6.76 (m, 1H), 6.27–6.23 (t, 2H,  $J = 9.0$  Hz), 2.34 (s, 6H), 1.30 (s, 12H). MALDI-TOF MS ( $\text{C}_{38}\text{H}_{37}\text{BN}_2\text{O}_2\text{S}$ )  $m/z$ : calcd for 596.589; found 596.309.

#### 2.2.13.

#### 5-(7-(10-(4-(Di-p-tolylamino)phenyl)-10H-phenothiazin-3-yl)benzo[c][1,2,5]thiadiazol-4-yl)-3-hexylthiophene-2-carbaldehyde (**15**)

The synthetic procedure for **15** was similar to that for **10**, except that compound **14** (0.56 g, 0.94 mmol) was used instead of compound **8**. The crude product was purified on silica gel chromatography using a petroleum ether/dichloromethane mixture (2/1 by volume) as eluent to afford a black red solid (0.52 g, 82.7%). <sup>1</sup>H NMR (CDCl<sub>3</sub>, 400MHz, δ/ppm): 10.09 (s, 1H), 8.05 (s, 1H), 8.01–7.99 (d, 1H, *J* = 7.4 Hz), 7.68–7.66 (d, 1H, *J* = 7.5 Hz), 7.63 (s, 1H), 7.60–7.57 (d, 1H, *J* = 8.7 Hz), 7.19–7.10 (m, 12H), 7.02–7.00 (d, 1H, *J* = 7.0 Hz), 6.92–6.89 (m, 1H), 6.84–6.81 (m, 1H), 6.45–6.43 (d, 1H, *J* = 8.6 Hz), 6.34–6.32 (d, 1H, *J* = 8.0 Hz), 3.06–3.02 (t, 2H, *J* = 7.5 Hz), 2.35 (s, 6H), 1.79–1.74 (m, 2H), 1.52–1.12 (m, 6H), 0.98–0.84 (m, 3H). <sup>13</sup>C NMR (100 MHz, CDCl<sub>3</sub>, δ/ppm): 182.01, 153.68, 148.42, 147.64, 145.05, 144.87, 144.00, 137.43, 133.52, 133.40, 131.42, 130.68, 130.48, 130.19, 128.02, 127.40, 126.99, 126.95, 126.65, 126.17, 125.42, 124.40, 122.81, 122.62, 120.13, 115.99, 115.71, 31.62, 31.45, 29.68, 29.08, 28.75, 22.59, 20.89, 14.06. MALDI-TOF MS (C<sub>49</sub>H<sub>42</sub>N<sub>4</sub>OS<sub>3</sub>) *m/z*: calcd for 799.079; found 798.289.

2.2.14. *(E)*-2-cyano-3-(5'-(10-(2-ethylhexyl)-10H-phenothiazin-3-yl)-4-hexyl-[2,2'-bithiophen]-5-yl)acrylic acid  
(**DXI**)

Compound **9** (0.23 g, 0.39 mmol), cyanoacetic acid (0.33 g, 3.90 mmol), and piperidine (0.19 mL) were dissolved in CHCl<sub>3</sub> (20 mL), and the solution was refluxed at 80 °C for 12 h under nitrogen atmosphere. Then the solution was poured into a diluted aqueous HCl (10 mL) solution and extracted with dichloromethane. The organic phase was dried over anhydrous MgSO<sub>4</sub>, and the solvent was removed by rotary evaporation. The crude product was purified using silica gel column chromatography (eluent: CH<sub>2</sub>Cl<sub>2</sub>/CH<sub>3</sub>OH = 50:1) to give a prunosus solid (0.18 g, 71.8%). <sup>1</sup>H NMR (DMSO, 400 MHz, δ/ppm): 8.27 (s, 1H), 7.57–7.56 (d, 1H, *J* = 3.2 Hz), 7.49 (s, 4H), 7.21–7.12 (m, 2H), 7.06–7.04 (d, 2H, *J* = 7.9 Hz), 6.97–6.96 (d, 1H, *J* = 7.1 Hz), 3.78 (s, 2H), 2.76 (s, 2H), 1.80 (s, 1H), 1.58 (s, 2H), 1.36–1.20 (m, 13H), 0.84–0.79 (m, 9H). <sup>13</sup>C NMR (100 MHz, CDCl<sub>3</sub>, δ/ppm): 168.64, 157.45, 147.55, 146.29, 145.99, 145.13, 144.80, 133.93, 128.86, 128.05, 127.75, 127.65, 127.32, 126.54, 125.57, 125.03, 124.78, 124.54,

123.46, 122.77, 116.09, 116.01, 51.19, 36.03, 31.53, 31.09, 30.78, 29.20, 29.02, 28.62, 24.09, 23.04, 22.54, 14.03, 13.97, 10.51. MALDI-TOF MS ( $C_{38}H_{42}N_2O_2S_3$ ) m/z: calcd for 654.947; found 654.247.

2.2.15.

*(E)-2-cyano-3-(5-(7-(10-(2-ethylhexyl)-10H-phenothiazin-3-yl)benzo[c][1,2,5]thiadiazol-4-yl)-3-hexylthiophen-2-yl)acrylic acid (DX2)*

The synthetic procedure for **DX2** was similar to that for **DX1**, except that compound **10** (0.20 g, 0.31 mmol) was used instead of compound **9**. The crude product was purified on silica gel chromatography (eluent:  $CH_2Cl_2/CH_3OH = 50:1$ ) to give a black red solid (0.20 g, 93.4%).  $^1H$  NMR (DMSO, 400 MHz,  $\delta/ppm$ ): 8.34 (s, 1H), 8.25–8.24 (d, 1H,  $J = 7.3$  Hz), 8.18 (s, 1H), 7.93–7.89 (m, 3H), 7.23–7.17 (m, 3H), 7.10–7.08 (d, 1H,  $J = 7.8$  Hz), 7.00–6.96 (m, 1H), 3.84 (s, 2H), 2.83 (s, 2H), 1.86 (s, 1H), 1.64 (s, 2H), 1.39–1.21 (m, 14H), 0.85–0.81 (m, 9H).  $^{13}C$  NMR (100 MHz,  $CDCl_3$ ,  $\delta/ppm$ ): 145.16, 130.74, 130.19, 128.25, 127.98, 127.86, 127.71, 127.23, 126.34, 125.97, 125.41, 123.79, 122.74, 116.11, 115.69, 51.21, 36.07, 31.61, 31.26, 30.84, 29.30, 29.08, 28.65, 24.12, 23.08, 22.58, 14.05, 13.99, 10.52. MALDI-TOF MS ( $C_{40}H_{40}N_4O_2S_3$ ) m/z: calcd for 706.982; found 706.315.

2.2.16.

*(E)-2-cyano-3-(5-(7-(10-(4-(di-*p*-tolylamino)phenyl)-10H-phenothiazin-3-yl)benzo[c][1,2,5]thiadiazol-4-yl)-3-hexylthiophen-2-yl)acrylic acid (DX3)*

The synthetic procedure for **DX3** was similar to that for **DX1**, except that compound **15** (0.20 g, 0.25 mmol) was used instead of compound **9**. The crude product was purified on silica gel chromatography (eluent:  $CH_2Cl_2/CH_3OH = 50:1$ ) to give a black solid (0.20 g, 91.0%).  $^1H$  NMR (DMSO, 400MHz,  $\delta/ppm$ ): 8.29 (s, 1H), 8.17–8.15 (d, 1H,  $J = 7.4$  Hz), 8.13 (s, 1H), 7.82–7.80 (d, 1H,  $J = 7.4$  Hz), 7.73 (s, 1H), 7.61–7.59 (d, 1H,  $J = 8.5$  Hz), 7.22–7.13 (m, 7H), 7.07–7.06 (d, 6H,  $J = 7.2$  Hz), 6.97–6.94 (m, 1H), 6.86–6.83 (m, 1H), 6.32–6.30 (d, 1H,  $J = 8.6$  Hz), 6.26–6.24 (d,

$^1\text{H}$ ,  $J = 8.0$  Hz), 2.81–2.78 (m, 2H), 2.28 (s, 6H), 1.62 (s, 2H), 1.29–1.21 (m, 6H), 0.85 (s, 3H).  $^{13}\text{C}$  NMR (100 MHz,  $\text{CDCl}_3$ ,  $\delta/\text{ppm}$ ): 148.32, 144.89, 143.90, 133.43, 132.80, 131.41, 130.41, 130.14, 127.91, 126.87, 126.60, 125.36, 122.88, 122.52, 119.44, 115.90, 115.61, 31.69, 31.14, 29.69, 29.22, 29.12, 22.59, 20.86, 14.08. MALDI-TOF MS ( $\text{C}_{52}\text{H}_{43}\text{N}_5\text{O}_2\text{S}_3$ )  $m/z$ : calcd for 866.125; found 865.307.

### 2.3. Instruments and characterizations

$^1\text{H}$  and  $^{13}\text{C}$  NMR spectra were measured on a Bruker Avance 400 instrument using tetramethylsilane (TMS;  $\delta = 0$  ppm) as internal standard. GC-MS spectrometric measurements were obtained on Agilent 7890-5975. MALDI-TOF mass spectrometric measurements were performed on Bruker Autoflex III. UV-Visible spectra of the dyes were measured on a Perkin-Elmer Lamada 25 spectrometer. The photoluminescence (PL) spectra were obtained using Perkin-Elmer LS-50 luminescence spectrometer. Electrochemical redox potentials were obtained by cyclic voltammetry (CV) using a three-electrode configuration and an electrochemistry workstation (ZAHNER ZENNIUM) at a scan rate of  $50 \text{ mV s}^{-1}$ . The working electrode was a glassy carbon electrode; the counter electrode was a Pt electrode, and saturated calomel electrode (SCE) was used as reference electrode. Tetrabutylammonium perchlorate (TBAP) 0.1 M was used as supporting electrolyte in nitrogen-purged anhydrous  $\text{CHCl}_3$ . Ferrocene/ferrocenium redox couple was used for potential calibration [5].

### 2.4. Fabrication and characterization of DSSCs

Fluorine-doped  $\text{SnO}_2$  conducting glass (FTO) were cleaned and immersed in aqueous 40 mM  $\text{TiCl}_4$  solution at  $70^\circ\text{C}$  for 30 min, then washed with water and ethanol, sintered at  $450^\circ\text{C}$  for 30 min. The  $\text{TiO}_2$  suspension was prepared from P25 (Degussa AG, Germany) [43] and 1 wt% magnesium acetate solution [44] on following a literature procedure. Then the paste was deposited onto the FTO glass by blade coating. Subsequently, a  $3 \mu\text{m}$  thick

200 nm particle sized TiO<sub>2</sub> scattering layer was deposited again by blade coating. The TiO<sub>2</sub>-coated FTO glass was sintered at 450 °C for 30 min, then treated with TiCl<sub>4</sub> solution at 70 °C for 30 min and calcined at 450 °C for 30 min again. After the film was cooled to room temperature, it was immersed into 0.5 mM dye solution with or without chenodeoxycholic acid (CDCA) (0.5mM) in the dark overnight. The sensitized electrode was then rinsed with ethanol and dried. A drop of electrolyte was deposited onto the surface of the electrode and a Pt foil counter electrode was clipped onto the top of the TiO<sub>2</sub> electrode to assemble a DSSC for photovoltaic performance measurements. The electrolyte consisted of 0.5 M LiI, 0.05 M I<sub>2</sub>, and 0.5 M 4-*tert*-butylpyridine (TBP) in 3-methoxypropionitrile and the efficient irradiated area of the cell was 0.2 cm<sup>2</sup>. The current density-voltage (*J*-*V*) curves were measured by a Keithley 2602 Source Meter under 100 mW cm<sup>-2</sup> standard AM 1.5G spectrum using a Sol 3A Oriel solar simulator. The incident light intensity was calibrated using a standard Si solar cell. The power conversion efficiency (*η*) of the DSSC is calculated from short-circuit photocurrent (*J*<sub>sc</sub>), the open-circuit photovoltage (*V*<sub>oc</sub>), the fill factor (*FF*) and the intensity of the incident light (*P*<sub>in</sub>) according to the following equation:

$$\eta = \frac{J_{sc} \text{ (mA cm}^{-2}\text{)} \times V_{oc} \text{ (V)} \times FF}{P_{in} \text{ (mW cm}^{-2}\text{)}}$$

The measurement of monochromatic incident photo-to-current conversion efficiency (IPCE) for the solar cell was also detected with a Zolix Solar Cell Scan 100 QE/IPCE measurement system.

### 3. Result and discussion

#### 3.1. Synthesis

The detailed synthetic routes of the three dyes **DX1**, **DX2** and **DX3** are shown in Scheme 1. The compound **2** and **6** were synthesized via Vilsmeier reaction. The compound **3** was synthesized by Stille coupling reaction. The

compound **1** and **13** were gained by two different bromination reactions, while the compound **11** was synthesized via an iodination reaction. The compound **12** was obtained through Ullmann coupling reaction. The compound **7** and **13** were transformed into the corresponding diboronic ester **8** and **14** via lithiation and subsequent quenching with 2-isopropoxy-4,4,5,5-tetramethyl-1,3,2-dioxaborolane, respectively. Then the compound **9**, **10** and **15** were synthesized by Suzuki reaction. Finally, the target dyes **DX1**, **DX2** and **DX3** were obtained via Knoevenagel condensation. The structures of the dyes **DX1**, **DX2** and **DX3** were verified by  $^1\text{H}$  NMR,  $^{13}\text{C}$  NMR, GC-MS and MALDI-TOF.

### 3.2. Photophysical properties

The UV-Vis absorption spectra of the dyes **DX1**, **DX2** and **DX3** in diluted ( $10^{-5}$  M) chloroform solutions are depicted in Fig. 1(a), and the corresponding data are listed in Table 1. The shorter-wavelength absorption peaks at ca. 300 nm and longer-wavelength absorption bands at ca. 450–600 nm could be assigned to the localized aromatic  $\pi$ - $\pi^*$  transitions of the conjugated aromatic moieties and intramolecular charge transfer (ICT) between the phenothiazine donor and the cyanoacrylic acid acceptor, respectively [42]. While the extra wavelength absorption bands (350–450 nm) in **DX2** and **DX3** appeared due to the introduction of BT moiety as a spacer [45]. The maximum absorption wavelengths ( $\lambda_{\text{max}}$ ) of **DX1**, **DX2** and **DX3** appeared at 494, 507 and 524 nm, and the corresponding molar extinction coefficients ( $\epsilon$ ) were  $2.62 \times 10^4$ ,  $2.21 \times 10^4$  and  $1.70 \times 10^4$   $\text{M}^{-1}\text{cm}^{-1}$ , respectively. In comparison with **DX1**, the ICT absorption peaks of **DX2** and **DX3** displayed red-shifts of 13 and 30 nm, respectively, which could be attributed to a better delocalization of electrons over the  $\pi$ -conjugated molecules, when the BT unit was used as an additional acceptor unit [46]. Moreover, a bathochromic shift of 17 nm of **DX3** compared to **DX2** in ICT absorption peak was observed, which might be interpreted on the basis of the increase in

the conjugation dimension for **DX3** with the participation of TPA unit, resulting in the enhanced  $\pi$ -electron density to the acceptor [47]. Simultaneously, the absorption onset was extended by 100 nm from 600 nm (**DX1**) to 700 nm (**DX2** and **DX3**) in a dilute solution. However, the  $\varepsilon$  values were decreased in **DX2** and **DX3**, which may lead to a drop in short-circuit photocurrent density ( $J_{sc}$ ) and photovoltaic performance.

In addition, as shown in Fig. 1(b), the maximum absorption peaks of three dyes on TiO<sub>2</sub> films were observed to severely blue-shift by 44, 87 and 25 nm with respect to those in solution for **DX1**, **DX2** and **DX3**, respectively, which could be mainly attributed to the H-type of aggregation and the partial deprotonation of carboxylic acid unit caused by the interaction between the dye and TiO<sub>2</sub> [48,49]. Apparently, **DX2** revealed a sharper hypsochromic shift than **DX1** and **DX3** in the absorption spectrum, indicating that **DX2** had a higher degree of H-type aggregation on the TiO<sub>2</sub> film [50]. Remarkably, a distinct red-shift of absorption onset from 700 nm (**DX1**) to 800 nm (**DX2** and **DX3**) could be seen in Fig. 1(b). Accordingly, the absorption spectra of **DX2** and **DX3** in solutions and on TiO<sub>2</sub> films showed a markedly broad profile, which was beneficial to light utilization [51].

### 3.3. Electrochemical properties

Cyclic voltammetry (CV) was carried out to estimate the possibility of electron injection and dye regeneration. As shown in Fig. 2 and Table 2, the first oxidation potentials ( $E_{ox}$ ), which corresponded to the highest occupied molecular orbital (HOMO) energy levels of **DX1**, **DX2** and **DX3**, were 0.96, 0.98 and 0.90 V, respectively, vs a normal hydrogen electrode (NHE), which were calibrated by addition of 0.65 V to the potential (vs. SCE) vs. Fc/Fc<sup>+</sup> by CV. All of them were more positive than the redox couple (I<sup>-</sup>/I<sub>3</sub><sup>-</sup>, 0.42 V), suggesting sufficient driving force for dye regeneration [52]. The similarity of HOMO energy levels of **DX1** and **DX2** was mainly attributed to their same donor unit, as the HOMO levels of compounds were mainly depended on the electron-donating moiety [53].

Additionally, the HOMO energy level of **DX3** was higher than those of **DX1** and **DX2**, which verified that the introduction of TPA unit led to stronger electron-donating property of **DX3**. Estimated from intersection of the normalized absorption and the emission spectrum ( $\lambda_{\text{int}}$ ) in Fig. 3, the zero-zero excitation energy ( $E_{0-0}$ ) values were 2.24, 2.27 and 2.25 V for **DX1**, **DX2** and **DX3**, respectively. The reduction potentials ( $E_{\text{red}}$  vs. NHE), corresponding to the lowest unoccupied molecular orbital (LUMO) energy level, were  $-1.28$ ,  $-1.29$  and  $-1.35$  V for **DX1**, **DX2** and **DX3**, respectively, calculated by  $E_{\text{ox}} - E_{0-0}$ . Apparently, the LUMO levels of the three dyes were more negative than the conduction band ( $E_{\text{cb}}$ ) of  $\text{TiO}_2$  (about  $-0.5$  V vs. NHE), indicative of thermodynamic feasibility for electron injection from the excited dyes into the  $\text{TiO}_2$  electrode [54]. Furthermore, the LUMO level of **DX3** was higher than the other dyes, which was beneficial for higher electron injection efficiency, namely, more sufficient electron flow from the excited dyes to the  $\text{TiO}_2$  surface [55].

#### 3.4. Density functional theory (DFT) calculations

To explain the structural properties of the dyes and understand the possibility of charge transfer from donor to acceptor on electronic excitation, the optimized structures of three dyes were calculated geometrically using the density functional theory (DFT) at the B3LYP/ 6-31G\* level. The optimized structures with torsion angles and electron densities of HOMOs and LUMOs of the dyes are shown in Table 3. In the optimized structures, the torsion angles between the hexylthiophene moiety and its adjoining aromatic units in three dyes were similar, but the changing tendency of torsion angles between the phenothiazine moiety and the adjacent units was in the order of **DX1** < **DX2** < **DX3**, indicating that the structure of **DX1** possesses relatively better planarity. In dye system, the planar structure can enhance the aromatic character of the heterocyclic atom, increasing the degree of electronic resonance between donor and acceptor moieties in the dye molecules and facilitating the electron transfer from

donor to cyanoacrylic acceptor. However, it increases the stacking of the dye molecules, resulting in more dye aggregation and electron recombination [56]. Thus, the electron transfer could be more effective in **DX1**, which corresponded to the emission spectra in Fig. 3. On the other hand, the electron densities of HOMOs in **DX1** and **DX2** were mainly localized over the phenothiazine moiety, whereas that in **DX3** was mostly localized over the TPA unit, which may due to the relatively strong electron-donating property of TPA unit. Additionally, the electron density of LUMO in **DX1** is mainly located on the cyanoacrylic segment and its adjoining hexylthiophene unit, suggesting the well-inductive electron tendency from phenothiazine donor to the cyanoacrylic acceptor. However, the electron densities of LUMOs in **DX2** and **DX3** were predominantly located on cyanoacrylic acceptor and extended to the hexylthiophene and BT moieties, facilitating the ICT between phenothiazine donor and the BT unit, and this in turn decreased the ICT between phenothiazine donor and the cyanoacrylic acceptor, and then reduced the utilization to long wave. From those observations, it is clearly evident that, in **DX1**, the HOMO-LUMO excitation induced by light irradiation could move the electron distribution from the phenothiazine moiety to the cyanoacrylic moiety more effectively, and the photo-induced electrons can be more efficiently transferred from the dye to the TiO<sub>2</sub> surface by the electric charge separation.

### 3.5. Photovoltaic properties of DSSCs

The photocurrent density-voltage ( $J$ - $V$ ) curves and the incident photon to current conversion efficiency (IPCE) spectra of DSSCs based on **DX1**, **DX2** and **DX3** with or without CDCA are shown in Fig. 4 and Fig. 5, with the detailed photovoltaic parameters summarized in Table 4. The IPCE value of **DX1** was over 60% in relatively narrow wavelength ranges from 400 to 550 nm, with a maximum IPCE value of 72% at 465 nm and an onset at 700 nm, showing a higher IPCE value than the other two dyes, which was in good accordance with the  $J_{sc}$  variation

obtained in  $J$ - $V$  measurements. On the other hand, **DX2** and **DX3** got maximum IPCE values of 38% at 470 nm and 47% at 465 nm, respectively, with the photocurrent signal up to ca. 800 nm. In accord with the UV-Vis absorption spectra in Fig. 1, **DX2** and **DX3** showed lower IPCE values compared to **DX1**.

As we all know, CDCA can work as an anti-aggregation compound to improve the performance in the DSSC devices [57,58]. Thus, the photovoltaic performances with CDCA as the co-adsorbent were studied in the DSSCs. Upon co-adsorption with 0.5 mM CDCA, The IPCE responses of DSSCs were remarkably increased compared to the dyes only. The plateaus of IPCE curves were lifted to 79%, 49% and 57%, and the  $J_{sc}$  increased to 11.46, 8.01 and 10.28 mA cm<sup>-2</sup> for **DX1**, **DX2** and **DX3**, respectively (Fig. 4). The remarkable enhancement of IPCE was attributed to the break-up of dye aggregation upon co-adsorption. The increased  $J_{sc}$  was due to the enhance injection efficiency resulting from relatively independent dye molecules arraying on TiO<sub>2</sub> surface [51], while the  $V_{oc}$  values were slightly increased, may due to the retardation of charge recombination arising from the prevention of  $\pi$ - $\pi$  stacking [59].

Consequently, the photovoltaic performances of DSSCs with CDCA were better than those without CDCA. As is well-known, a high  $J_{sc}$  and  $V_{oc}$  can lead to a high PCE. Despite the panchromatic responses of **DX2** and **DX3**, they showed lower  $J_{sc}$  values because of the lower IPCE values resulting from the lower  $\epsilon$  values with respect to **DX1**. As a result, the **DX1**-based DSSC with 0.5 mM CDCA as the co-adsorbent exhibited the best PCE of 5.69%, and the DSSCs based on **DX2** and **DX3** with CDCA obtained PCEs of 3.43% and 4.41%, respectively, while the reference ruthenium dye of **N719** gives the PCE of 6.56% at the same conditions.

### 3.6. Electrochemical impedance spectroscopy studies

To further understand the relationship between the charge transfer process and photovoltaic properties of the

DSSCs, electrochemical impedance spectroscopy (EIS) was employed under a forward bias of  $-0.65$  V in the dark. The Nyquist plots for the DSSCs based on **DX1**, **DX2** and **DX3** are displayed in Fig. 6 (a). The first semicircle ( $R_{ce}$ ) is attributed to charge transfer at the counter electrode/electrolyte interface, while the second semicircle ( $R_{rec}$ ) is accorded to charge transfer at the  $TiO_2$ /dye/electrolyte interface [60]. The similar  $R_{ce}$  values (for **DX1**, **DX2** and **DX3**) were probably due to the same counter electrode and electrolyte. A large  $R_{rec}$  means a small dark current and a low charge recombination rate [61]. The  $R_{rec}$  values for **DX1**, **DX2** and **DX3** were estimated to be 90, 65 and 49  $\Omega$ , respectively, as shown in Table 4. Obviously, the  $R_{rec}$  value of **DX1** was much larger than the other two dyes, which could restrain the charge recombination between injected electron and electron acceptor ( $I_3^-$ ) in the electrolyte, thereby contributing to the  $V_{oc}$  [53].

On the other hand, the Bode plots for the DSSCs based on **DX1**, **DX2** and **DX3** are shown in Fig. 6 (b). The peaks located at the high-frequency (right) and middle-frequency (left) respectively correspond to the small semicircle (left) and large semicircle (right) in the Nyquist plots (Fig. 6 (a)). The reciprocal of the peak frequency for the middle-frequency peak is regarded as the electron lifetime since it represents the charge transfer process at the  $TiO_2$ /dye/electrolyte interface. So the trend of electron lifetimes was in the order of **DX1** > **DX2** > **DX3**, which was well in accordance with the changing tendencies of  $V_{oc}$  values obtained in  $J-V$  curves. Evidently, the longer electron lifetime of **DX1** compared to the other two dyes could suppress the generation of dark current and reduce electron recombination more effectively, resulting in a higher  $V_{oc}$  in **DX1**-based device [50].

#### 4. Conclusions

In summary, we reported the design and synthesis of three novel phenothiazine-based dyes **DX1**, **DX2** and **DX3**. By replacing the thiophene unit with the strong electron-withdrawing BT moiety, **DX2** and **DX3** displayed

remarkable responses in the NIR region as well as a panchromatic response in DSSCs. However, the lower  $J_{sc}$  resulted from the lower IPCE values led to lower photovoltaic performances in **DX2**- and **DX3**-based devices compared to the **DX1**-based one. Additionally, with the introduction of strong electron-donating TPA unit, the dye aggregation was reduced and electron injection efficiency was increased, thus the  $J_{sc}$  of the **DX3**-based device was increased, resulting in a higher PCE in the **DX3**-based device with respect to the **DX2**-based one. Upon co-adsorption with 0.5 mM CDCA, The photovoltaic performances of DSSCs were remarkably increased compared to the dyes only. Consequently, the device based on **DX1** with 0.5 mM CDCA obtained the highest PCE of 5.69%, and the cells based on **DX2** and **DX3** with 0.5 mM CDCA got PCEs of 3.43% and 4.41%, respectively, while the reference ruthenium dye of **N719** gives the PCE of 6.56% at the same conditions. The researches on structure tuning of phenothiazine-based dyes enrich their application in DSSCs. And we believe that with further optimization to the molecular structure and the device, the photovoltaic performances of phenothiazine-based dyes can be improved tremendously.

### Acknowledgments

This work was supported by the National Nature Science Foundation of China (51173154), and Hunan Provincial Natural Science Foundation of China (13JJ2025).

### References

- (1) O'Regan B, Grätzel M. A low-cost, high-efficiency solar cell based on dye-sensitized colloidal TiO<sub>2</sub> films. *Nature* **1991**;353:737-40.
- (2) Hagfeldt A, Grätzel M. Light-induced redox reactions in nanocrystalline systems. *Chem Rev* **1995**;95:49-68.
- (3) Wang Z, Cui Y, Dan-oh Y, Kasada C, Shinpo A, Hara K. Thiophene-functionalized coumarin dye for efficient

dye-sensitized solar cells: electron lifetime improved by coadsorption of deoxycholic acid. *J Phys Chem C* **2007**;111:7224-30.

- (4) Yang H, Yen Y, Hsu Y, Chou H, Lin JT. Organic dyes incorporating the dithieno[3,2-b:2',3'-d]thiophene moiety for efficient dye-sensitized solar cells. *Org Lett* **2009**;12:16-9.
- (5) Tian H, Yang X, Chen R, Zhang R, Hagfeldt A, Sun L. Effect of different dye baths and dye-structures on the performance of dye-sensitized solar cells based on triphenylamine dyes. *J Phys Chem C* **2008**;112:11023-33.
- (6) Mishra A, Fischer MKR, Bäuerle P. Metal-free organic dyes for dye-sensitized solar cells: from structure: property relationships to design rules. *Angew Chem Int Edit* **2009**;48:2474-99.
- (7) Péchy P, Renouard T, Zakeeruddin SM, Humphry-Baker R, Comte P, Liska P, Cevey L, Costa E, Shklover V, Spiccia L, Deacon GB, Bignozzi CA, Grätzel M. Engineering of efficient panchromatic dyes for nanocrystalline TiO<sub>2</sub>-based solar cells. *J Am Chem Soc* **2001**;123:1613-24.
- (8) Aswani Yella, Hsuan-Wei Lee, Hoi Nok Tsao, Chenyi Yi, Aravind Kumar Chandiran, Md. Khaja Nazeeruddin, Eric Wei-Guang Diao, Chen-Yu Yeh, Shaik M Zakeeruddin, Michael Grätzel. Porphyrin-sensitized solar cells with cobalt (II/III) - based redox electrolyte exceed 12 percent efficiency. *Science* **2011**;334:629-34.
- (9) Yella A, Mai C, Zakeeruddin SM, Chang S, Hsieh C, Yeh C, Grätzel M. Molecular engineering of push - pull porphyrin dyes for highly efficient dye-sensitized solar cells: the role of benzene spacers. *Angew Chem Int Edit* **2014**;53:2973-7.
- (10) Mathew S, Yella A, Gao P, Humphry-Baker R, Curchod BFE, Ashari-Astani N, Tavernelli I, Rothlisberger U, Nazeeruddin MK, Grätzel M. Dye-sensitized solar cells with 13% efficiency achieved through the molecular engineering of porphyrin dyes. *Nat Chem* **2014**;6:242-7.
- (11) Climent C, Cabau L, Casanova D, Wang P, Palomares E. Molecular dipole, dye structure and electron lifetime relationship in efficient dye sensitized solar cells based on donor -  $\pi$  - acceptor organic dyes. *Org Electron* **2014**;15:3162-72.
- (12) Chen B, Chen D, Chen C, Hsu C, Hsu H, Wu K, Liu S, Chou P, Chi Y. Donor-acceptor dyes with fluorine substituted

phenylene spacer for dye-sensitized solar cells. *J Mater Chem* **2011**;21:1937-45.

(13) Ren X, Jiang S, Cha M, Zhou G, Wang Z. Thiophene-bridged double D- $\pi$ -A dye for efficient dye-sensitized solar cell.

*Chem Mater* **2012**;24:3493-9.

(14) Hua Y, Chang S, Huang D, Zhou X, Zhu X, Zhao J, Chen T, Wong W, Wong W. Significant improvement of dye-sensitized solar cell performance using simple phenothiazine-based dyes. *Chem Mater* **2013**;25:2146-53.

(15) Cao D, Peng J, Hong Y, Fang X, Wang L, Meier H. Enhanced performance of the dye-sensitized solar cells with phenothiazine-based dyes containing double D-A branches. *Org Lett* **2011**;13:1610-3.

(16) Koumura N, Wang Z, Mori S, Miyashita M, Suzuki E, Hara K. Alkyl-functionalized organic dyes for efficient molecular photovoltaics. *J Am Chem Soc* **2006**;128:14256-7.

(17) Horiuchi T, Miura H, Sumioka K, Uchida S. High efficiency of dye-sensitized solar cells based on metal-free indoline dyes. *J Am Chem Soc* **2004**;126:12218-9.

(18) Zang X, Xu Y, Iqbal Z, Huang Z, Kuang D, Wang L, Meier H, Li Y, Cao D. Synthesis and photovoltaic performance of dihydrodibenzoazepine-based dyes with additional lateral anchor. *Dyes Pigments* **2013**;99:1072-81.

(19) Hart AS, K. C. CB, Subbaiyan NK, Karr PA, D Souza F. Phenothiazine-sensitized organic solar cells: effect of dye anchor group positioning on the cell performance. *ACS Appl Mat Inter* **2012**;4:5813-20.

(20) Li H, Hou Y, Yang Y, Tang R, Chen J, Wang H, Han H, Peng T, Li Q, Li Z. Attempt to improve the performance of pyrrole-containing dyes in dye sensitized solar cells by adjusting isolation groups. *ACS Appl Mat Inter* **2013**;5:12469-77.

(21) Liang M, Xu Y, Wang X. Synthesis of triarylamine dyes containing secondary electron-donating groups and application in the dye-sensitized solar cells. *Acta Chim Sinica* **2011**;69:2092.

(22) Ning Z, Fu Y, Tian H. Improvement of dye-sensitized solar cells: what we know and what we need to know. *Energy Environ Sci* **2010**;3:1170-81.

- (23) Liu L, Chen J, Ku Z, Li X, Han H. Unsymmetrical squaraine dyes containing auxiliary arylamine donor for NIR-harvesting on dye-sensitized solar cell. *Dyes Pigments* **2014**;106:128-35.
- (24) Xie Z, Midya A, Loh KP, Adams S, Blackwood DJ, Wang J, Zhang X, Chen Z. Highly efficient dye-sensitized solar cells using phenothiazine derivative organic dyes. *Prog Photovoltaics* **2010**;18:573-81.
- (25) Cao D, Peng J, Hong Y, Fang X, Wang L, Meier H. Enhanced performance of the dye-sensitized solar cells with phenothiazine-based dyes containing double D-A branches. *Org Lett* **2011**;13:1610-3.
- (26) Chang YJ, Chou P, Lin Y, Watanabe M, Yang C, Chin T, Chow TJ. Organic dyes containing oligo-phenothiazine for dye-sensitized solar cells. *J Mater Chem* **2012**;22:21704-12.
- (27) Chen C, Liao J, Chi Z, Xu B, Zhang X, Kuang D, Zhang Y, Liu S, Xu J. Metal-free organic dyes derived from triphenylethylene for dye-sensitized solar cells: tuning of the performance by phenothiazine and carbazole. *J Mater Chem* **2012**;22:8994-9005.
- (28) Kim SH, Kim HW, Sakong C, Namgoong J, Park SW, Ko MJ, Lee CH, Lee WI, Kim JP. Effect of five-membered heteroaromatic linkers to the performance of phenothiazine-based dye-sensitized solar cells. *Org Lett* **2011**;13:5784-7.
- (29) Tan H, Pan C, Wang G, Wu Y, Zhang Y, Yu G, Zhang M. A comparative study on properties of two phenoxazine-based dyes for dye-sensitized solar cells, *Dyes Pigments* **2014**;101:67-73.
- (30) Tian H, Yang X, Chen R, Pan Y, Li L, Hagfeldt A, Sun L. Phenothiazine derivatives for efficient organic dye-sensitized solar cells. *Chem Commun* **2007**;3741-3.
- (31) Wu W, Yang J, Hua J, Tang J, Zhang L, Long Y, Tian H. Efficient and stable dye-sensitized solar cells based on phenothiazine dyes with thiophene units. *J Mater Chem* **2010**;20:1772-9.
- (32) Wu Y, Zhu W. Organic dyes from D- $\pi$ -A to D-A- $\pi$ -A: effect of the internal electron-withdrawing units on molecular absorption, energy levels and photovoltaic performances. *Chem Soc Rev* **2013**;42:2039-58.

- (33) Li H, Yang L, Tang R, Hou Y, Yang Y, Wang H, Han H, Qin J, Li Q, Li Z. Organic dyes incorporating N-functionalized pyrrole as conjugated bridge for dye-sensitized solar cells: convenient synthesis, additional withdrawing group on the  $\pi$ -bridge and the suppressed aggregation. *Dyes Pigments* **2013**;99:863-70.
- (34) Haid S, Marszalek M, Mishra A, Wielopolski M, Teuscher J, Moser J, Humphry-Baker R, Zakeeruddin SM, Grätzel M, Bäuerle P. Significant improvement of dye-sensitized solar cell performance by small structural modification in  $\pi$ -conjugated donor-acceptor dyes. *Adv Funct Mater* **2012**;22:1291-302.
- (35) Wu Y, Marszalek M, Zakeeruddin SM, Zhang Q, Tian H, Grätzel M, Zhu W. High-conversion-efficiency organic dye-sensitized solar cells: molecular engineering on D-A- $\pi$ -A featured organic indoline dyes. *Energy Environ Sci* **2012**;5:8261-72.
- (36) Li J, Chen C, Lee C, Chen S, Lin T, Tsai H, Ho K, Wu C. Unsymmetrical squaraines incorporating the thiophene unit for panchromatic dye-sensitized solar cells. *Org Lett* **2010**;12:5454-7.
- (37) Kim J, Choi H, Lee J, Kang M, Song K, Kang SO, Ko J. A polymer gel electrolyte to achieve  $\geq 6\%$  power conversion efficiency with a novel organic dye incorporating a low-band-gap chromophore. *J Mater Chem* **2008**;18:5223-9.
- (38) Tang Z, Lei T, Jiang K, Song Y, Pei J. Benzothiadiazole containing D- $\pi$ -A conjugated compounds for dye-sensitized solar cells: synthesis, properties, and photovoltaic performances. *Chem-Asian J* **2010**;5:1911-7.
- (39) Liang Y, Peng B, Liang J, Tao Z, Chen J. Triphenylamine-based dyes bearing functionalized 3,4-propylenedioxythiophene linkers with enhanced performance for dye-sensitized solar cells. *Org Lett* **2010**;12:1204-7.
- (40) Liang Y, Peng B, Chen J. Correlating dye adsorption behavior with the open-circuit voltage of triphenylamine-based dye-sensitized solar cells. *J Phys Chem C* **2010**;114:10992-8.
- (41) Huang Y, Li L, Peng X, Peng J, Cao Y. Solution processed small molecule bulk heterojunction organic photovoltaics based on a conjugated donor-acceptor porphyrin. *J Mater Chem* **2012**;22:21841.
- (42) Hung W, Liao Y, Hsu C, Chou H, Lee T, Kao W, Lin JT. High-performance dye-sensitized solar cells based on

phenothiazine dyes containing double anchors and thiophene spacers. *Chem-Asian J* **2014**;9:357-66.

(43) Kalyanasundaram K和GT. Applications of functionalized transition metal complexes in photonic and optoelectronic devices. *Coord Chem Rev* **1998**;177:347-414.

(44) Kumara GRA, Kaneko S, Konno A, Okuya M, Murakami K, Onwona-agyeman B, Tennakone K. Large area dye-sensitized solar cells: material aspects of fabrication. *Prog Photovoltaics* **2006**;14:643-51.

(45) Katono M, Wielopolski M, Marszalek M, Bessho T, Moser J, Humphry-Baker R, Zakeeruddin SM, Grätzel M. Effect of extended  $\pi$ -conjugation of the donor structure of organic D - A -  $\pi$  - A dyes on the photovoltaic performance of dye-sensitized solar cells. *J Phys Chem C* **2014**;118:16486-93.

(46) Wang X, Yang J, Yu H, Li F, Fan L, Sun W, Liu Y, Koh ZY, Pan J, Yim W, Yan L, Wang Q. A benzothiazole - cyclopentadithiophene bridged D - A -  $\pi$  - A sensitizer with enhanced light absorption for high efficiency dye-sensitized solar cells. *Chem Commun* **2014**;50:3965.

(47) Bodedla GB, Thomas KRJ, Li C, Ho K. Functional tuning of phenothiazine-based dyes by a benzimidazole auxiliary chromophore: an account of optical and photovoltaic studies. *RSC Adv* **2014**;4:53588-601.

(48) Chen R, Yang X, Tian H, Sun L. Tetrahydroquinoline dyes with different spacers for organic dye-sensitized solar cells. *J Photoch Photobio A* **2007**;189:295-300.

(49) Lin L, Tsai C, Wong K, Huang T, Hsieh L, Liu S, Lin H, Wu C, Chou S, Chen S, Tsai A. Organic dyes containing coplanar diphenyl-substituted dithienosilole core for efficient dye-sensitized solar cells. *J Org Chem* **2010**;75:4778-85.

(50) Huang Z, Feng H, Zang X, Iqbal Z, Zeng H, Kuang D, Wang L, Meier H, Cao D. Dithienopyrrolobenzothiadiazole-based organic dyes for efficient dye-sensitized solar cells. *J Mater Chem A* **2014**;2:15365.

(51) Zhu W, Wu Y, Wang S, Li W, Li X, Chen J, Wang Z, Tian H. Organic D-A- $\pi$ -A solar cell dyes with improved stability and spectral response. *Adv Funct Mater* **2011**;21:756-63.

- (52) Liu X, Cao Z, Huang H, Liu X, Tan Y, Chen H, Pei Y, Tan S. Novel D - D -  $\pi$ -A organic dyes based on triphenylamine and indole-derivatives for high performance dye-sensitized solar cells. *J Power Sources* **2014**;248:400-6.
- (53) Wang D, Ying W, Zhang X, Hu Y, Wu W, Hua J. Near-infrared absorbing isoindigo dyes: Synthesis and performance for dye-sensitized solar cells. *Dyes Pigments* **2015**;112:327-34.
- (54) Hagfeldt A, Grätzel M. Light-induced redox reactions in nanocrystalline systems. *Chem Rev* **1995**;95:49-68.
- (55) Hara K, Sato T, Katoh R, Furube A, Ohga Y, Shinpo A, Suga S, Sayama K, Sugihara H, Arakawa H. Molecular design of coumarin dyes for efficient dye-sensitized solar cells. *J Phys Chem B* **2002**;107:597-606.
- (56) Lee W, Yuk SB, Choi J, Kim HJ, Kim HW, Kim SH, Kim B, Ko MJ, Kim JP. The effects of the number of anchoring groups and N-substitution on the performance of phenoxazine dyes in dye-sensitized solar cells. *Dyes Pigments* **2014**;102:13-21.
- (57) Hara K, Dan-oh Y, Kasada C, Ohga Y, Shinpo A, Suga S, Sayama K, Arakawa H. Effect of additives on the photovoltaic performance of coumarin-dye-sensitized nanocrystalline TiO<sub>2</sub> solar cells. *Langmuir* **2004**;20:4205-10.
- (58) Wang Z, Cui Y, Dan-oh Y, Kasada C, Shinpo A, Hara K. Molecular design of coumarin dyes for stable and efficient organic dye-sensitized solar cells. *J Phys Chem C* **2008**;112:17011-7.
- (59) Neale NR, Kopidakis N, van de Lagemaat J, Grätzel M, Frank AJ. Effect of a coadsorbent on the performance of dye-sensitized TiO<sub>2</sub> solar cells: shielding versus band-edge movement. *J Phys Chem B* **2005**;109:23183-9.
- (60) Wang Q, Moser J, Grätzel M. Electrochemical impedance spectroscopic analysis of dye-sensitized solar cells. *J Phys Chem B* **2005**;109:14945-53.
- (61) Cheng M, Yang X, Li J, Chen C, Zhao J, Wang Y, Sun L. Dye-sensitized solar cells based on a donor - acceptor system with a pyridine cation as an electron-withdrawing anchoring group. *Chem Eur J* **2012**;18:16196-202.

**Captions for Tables, Scheme and Figures**

Table 1 Maximum absorption and emission data of the dyes **DX1**, **DX2** and **DX3**.

Table 2 Electrochemical data of the dyes **DX1**, **DX2** and **DX3**.

Table 3 Optimized structures, torsion angles and electronic distributions in HOMO and LUMO levels of the dyes **DX1**, **DX2** and **DX3**.

Table 4 Photovoltaic performance parameters of DSSCs based on the dyes **DX1**, **DX2** and **DX3**.

Scheme 1. Synthetic routes and molecular structures of the three dyes **DX1**, **DX2** and **DX3**.

Fig. 1. Absorption spectra of **DX1**, **DX2** and **DX3** in diluted  $\text{CHCl}_3$  solutions (a) and on  $\text{TiO}_2$  thin-films (b).

Fig. 2. Cyclic voltammogram (a) and energy level diagram (b) of the dyes **DX1**, **DX2** and **DX3**.

Fig. 3. Emission spectra of the dyes **DX1**, **DX2** and **DX3** in diluted  $\text{CHCl}_3$  solutions.

Fig. 4. IPCE action spectra for the DSSCs based on the **DX1**, **DX2** and **DX3** with or without CDCA on dye-sensitized transparent  $\text{TiO}_2$  films.

Fig. 5.  $J-V$  curves for DSSCs with the dyes **DX1**, **DX2** and **DX3** with or without CDCA under AM 1.5 simulated sunlight ( $100 \text{ mW cm}^{-2}$ ) illumination.

Fig. 6. EIS Nyquist plots (a) and Bode plots (b) for DSSCs based on **DX1**, **DX2** and **DX3** measured under  $-0.65 \text{ V}$  bias in the dark.

Table 1

Maximum absorption and emission data of the dyes **DX1**, **DX2** and **DX3**

Dye	$\lambda_{\text{abs}}/\text{nm}$ ( $\epsilon(\times 10^4 \text{ M}^{-1} \text{ cm}^{-1})^{\text{a}}$ )	$\lambda_{\text{max}}/\text{nm}$ (on $\text{TiO}_2$ ) <sup>b</sup>	$\lambda_{\text{em}}/(\text{nm})^{\text{c}}$
<b>DX1</b>	494(2.62)	450	641
<b>DX2</b>	420(1.89)	507(2.21)	582
<b>DX3</b>	422(1.80)	524(1.70)	572

<sup>a</sup> Maximum absorption in  $\text{CHCl}_3$  solution ( $10^{-5} \text{ M}$ ) at  $25^\circ \text{C}$ .<sup>b</sup> Maximum absorption on  $\text{TiO}_2$  film.<sup>c</sup> Maximum emission of the dyes in  $\text{CHCl}_3$  solution ( $10^{-5} \text{ M}$ ) at  $25^\circ \text{C}$ .

Table 2

Electrochemical data of the dyes **DX1**, **DX2** and **DX3**.

Dye	$\lambda_{\text{int}}/\text{nm}$	$E_{0-0}/\text{eV}$	$E_{\text{ox}}/\text{V}$ vs NHE	$E_{\text{red}}/\text{V}$ vs NHE	$E_{\text{gap}}/\text{V}$
<b>DX1</b>	554	2.24	0.96	-1.28	0.78
<b>DX2</b>	545	2.27	0.98	-1.29	0.79
<b>DX3</b>	552	2.25	0.90	-1.35	0.85

 $E_{0-0}$  values were calculated from intersection of the normalized absorption and the emission spectrum ( $\lambda_{\text{int}}$ ):  $E_{0-0} = 1240/\lambda_{\text{int}}$ . The firstoxidation potential (vs NHE),  $E_{\text{ox}}$  was measured in  $\text{CHCl}_3$  and calibrated by addition of 0.65 V to the potential vs  $\text{Fc}/\text{Fc}^+$ . The reductionpotential,  $E_{\text{red}}$ , was calculated from  $E_{\text{ox}} - E_{0-0}$ .  $E_{\text{gap}}$  is the energy gap between the  $E_{\text{red}}$  of dye and the conductive band level of  $\text{TiO}_2$  (-0.5

V vs NHE).

Table 3

Optimized structures, torsion angles and electronic distributions in HOMO and LUMO levels of the dyes **DX1**, **DX2** and **DX3**.

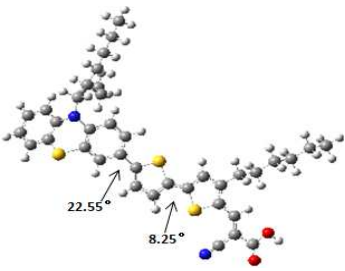
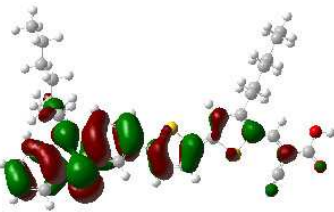
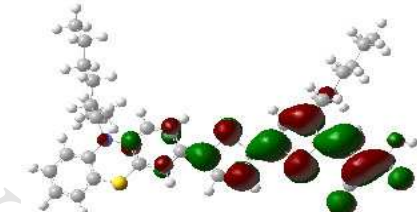
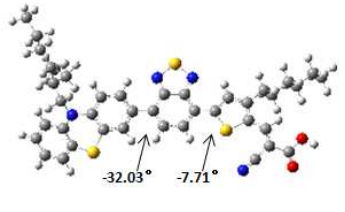
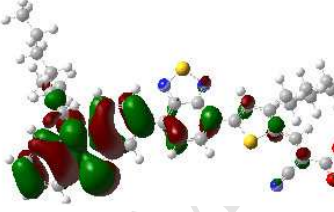
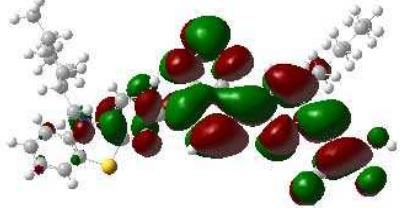
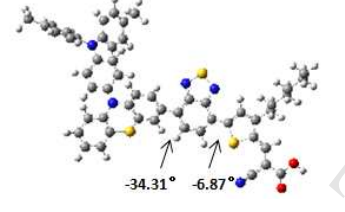
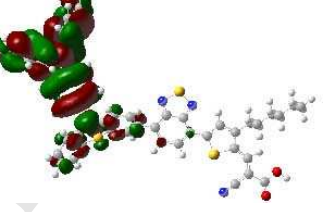
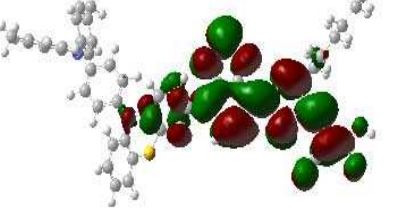
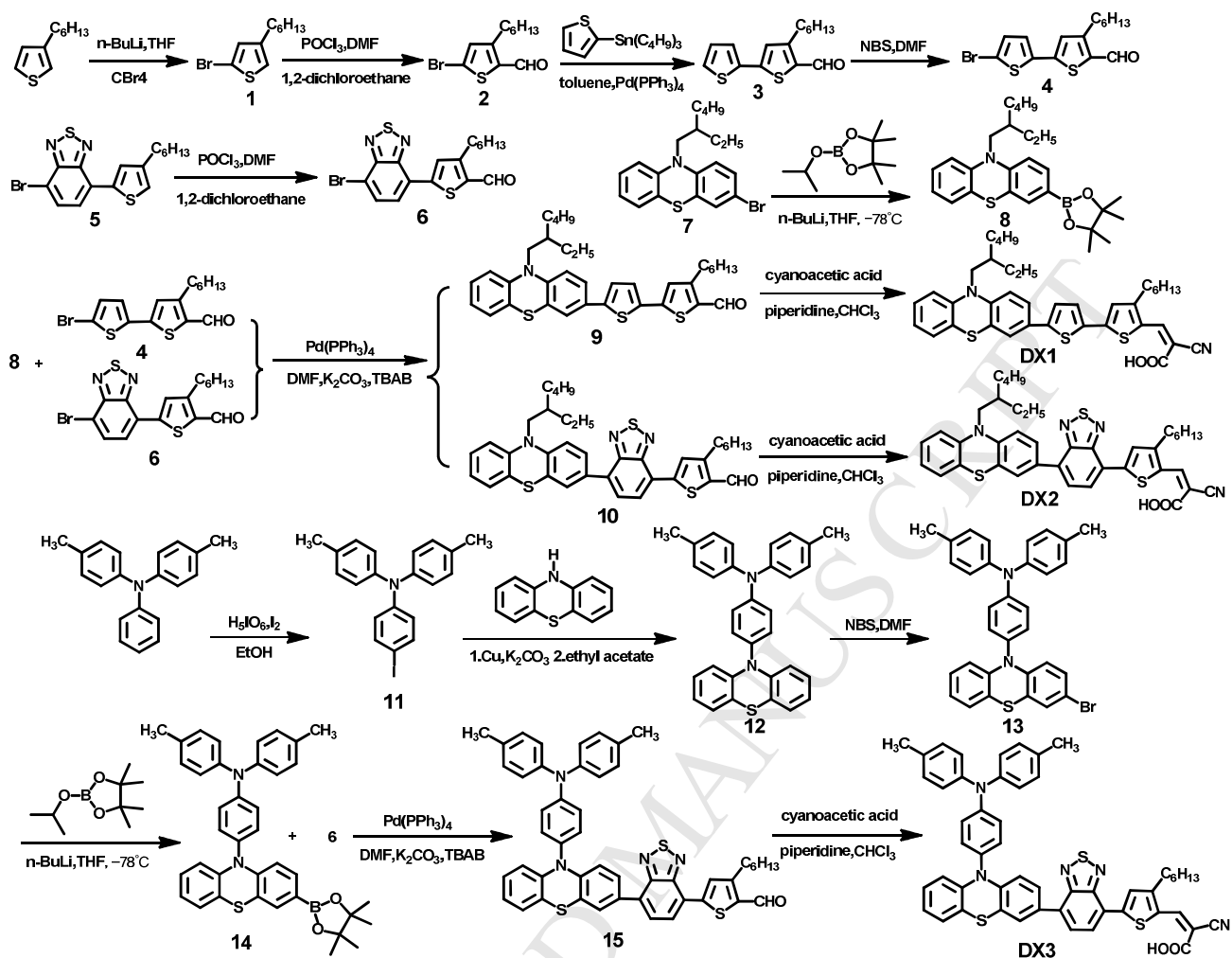
Dye	Optimized structure	HOMO	LUMO
<b>DX1</b>			
<b>DX2</b>			
<b>DX3</b>			

Table 4

Photovoltaic performance parameters of DSSCs based on the dyes **DX1**, **DX2** and **DX3**.

Dye	Co-adsorbent	$J_{sc}$ (mA cm <sup>-2</sup> )	$V_{oc}$ (V)	FF	$\eta$ (%)	$R_{rec}$
<b>DX1</b>	—	10.35	0.67	0.72	5.00	90
<b>DX1</b>	0.5mM CDCA	11.46	0.69	0.72	5.69	—
<b>DX2</b>	—	5.78	0.61	0.74	2.60	65
<b>DX2</b>	0.5mM CDCA	8.01	0.62	0.70	3.43	—
<b>DX3</b>	—	8.46	0.59	0.70	3.54	49
<b>DX3</b>	0.5mM CDCA	10.28	0.61	0.70	4.41	—
<b>N719</b>	—	12.59	0.73	0.72	6.56	—

Scheme 1. Synthetic routes and molecular structures of the three dyes **DX1**, **DX2** and **DX3**.

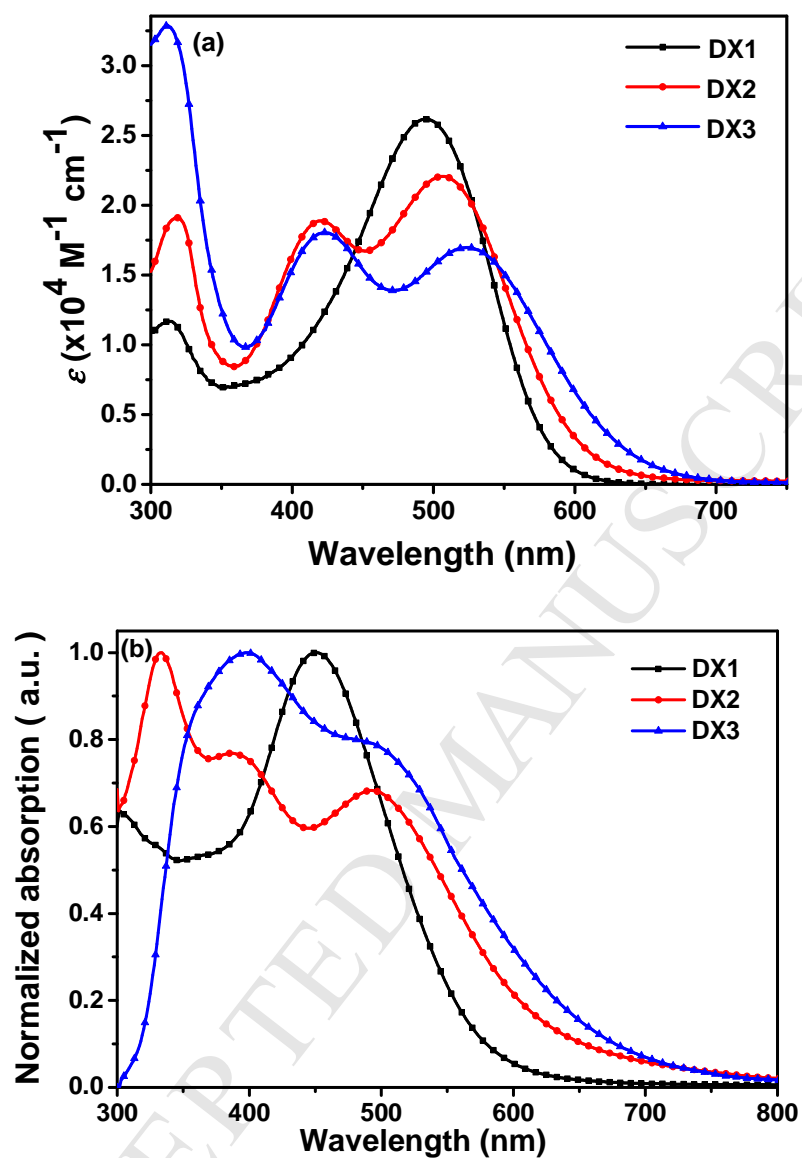


Fig. 1. Absorption spectra of **DX1**, **DX2** and **DX3** in diluted  $\text{CHCl}_3$  solutions (a) and on  $\text{TiO}_2$  thin-films (b).

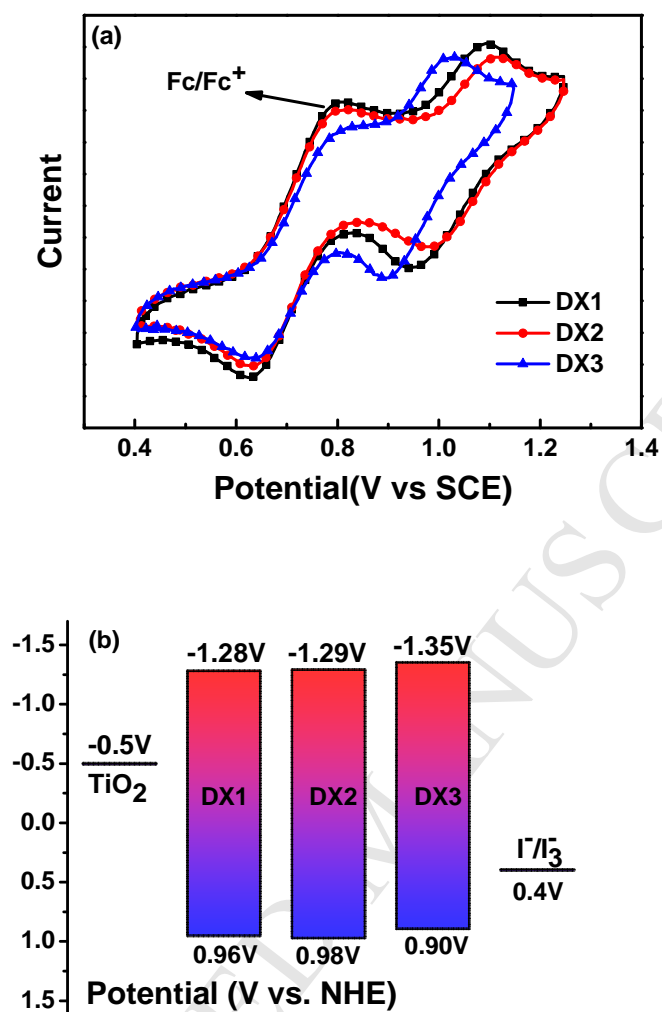


Fig. 2. Cyclic voltammogram (a) and energy level diagram (b) of the dyes **DX1**, **DX2** and **DX3**.

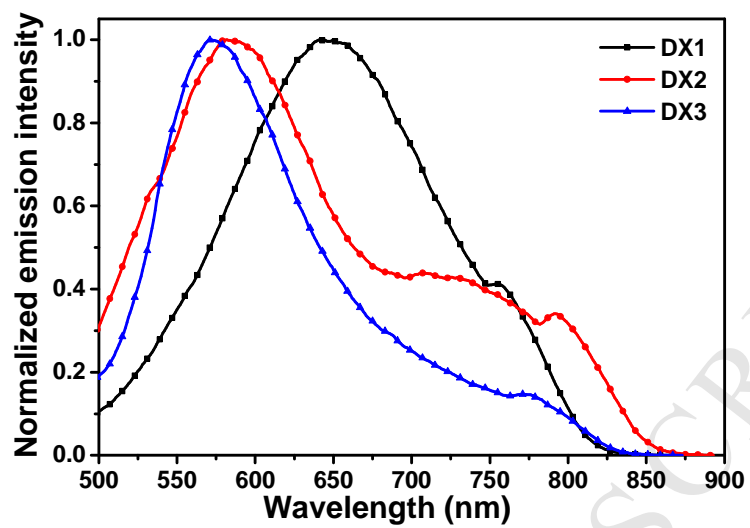


Fig. 3. Emission spectra of the dyes **DX1**, **DX2** and **DX3** in diluted  $\text{CHCl}_3$  solutions.

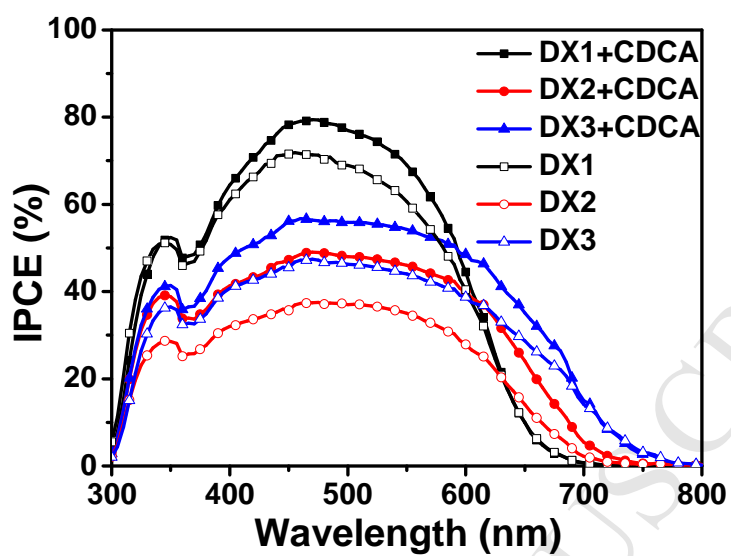


Fig. 4. IPCE action spectra for the DSSCs based on the **DX1**, **DX2** and **DX3** with or without CDCA on dye-sensitized transparent  $\text{TiO}_2$  films.

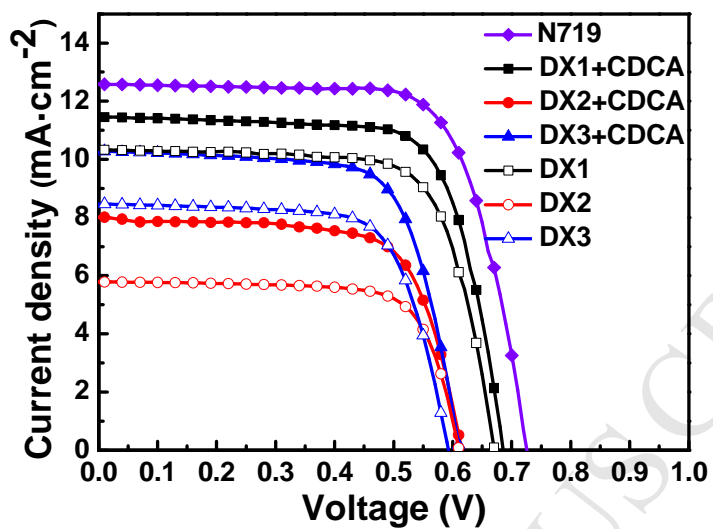


Fig. 5.  $J$ - $V$  curves for DSSCs with the dyes **DX1**, **DX2** and **DX3** with or without CDCA under AM 1.5 simulated sunlight ( $100 \text{ mW cm}^{-2}$ ) illumination.

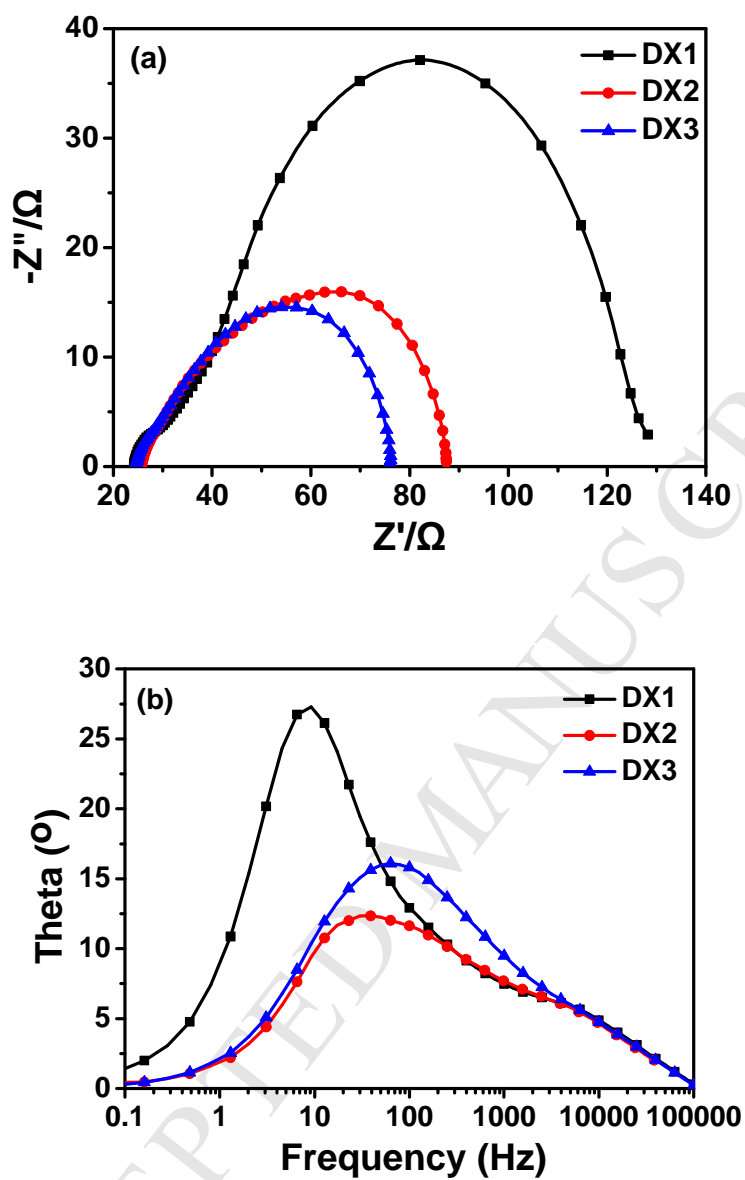


Fig. 6. EIS Nyquist plots (a) and Bode plots (b) for DSSCs based on **DX1**, **DX2** and **DX3** measured under  $-0.65$  V bias in the dark.

### Highlights

- (1) Three novel phenothiazine-based dyes were synthesized for DSSCs.
- (2) The DSSC device based on the dye **DX1** obtained the highest PCE of 5.69%.
- (3) The dyes **DX2** and **DX3** display broad spectra responses.